Chemical Exfoliating 2D Molybdenum Oxide Nanoflakes for Cancer Cells Photothermal Ablation

Tao Bao [1, 2], Xiaoli Peng [1], Wenyan Yin [2], Jinhui Lin [1,*]

[1]Chengdu University of Technology, College of Materials and Chemistry & Chemical Engineering, Chengdu, 610059, China

[2]CAS Key Laboratory for Biomedical Effects of Nanomaterials and Nanosafety, Institute of High Energy Physics, Chinese Academy of Sciences, Beijing 100049, China

[a]baotao@ihep.ac.cn

Abstract

Plasmonic materials have drawn emerging interest in modern science and technology, especially in optical systems and photo-mediated biomedical fields. Herein, a novel type of 2D nanomaterial, Molybdenum oxide nanoflakes (MoO_{3-x} NFs) were synthesized through hydrothermal and mechanical exfoliating method. The obtained oxygen vacancy-rich MoO_{3-x} nanoflakes display intense absorption in a wide range attributed to the localized surface plasmon resonances, which can be tuned from the visible to the near-infrared region. Upon a 808 nm laser irradiation, MoO_{3-x} NFs can possess intrinsic NIR-induced hyperthermia and are able to kill cancer cells. The enhanced NIR absorption, low cytotoxicity of MoO3-x NFs make them potential photothermal agent. This study will benefit future design and optimization of photothermal agents for biomedical application.

Keywords

Plasmonic, photo-mediated, hyperthermia, photothermal agent.

1. Introduction

Plasmonic materials exhibit certain physical and chemical properties have shown great promise for exploitation as a new generation of functional materials[1-3]. Extraordinary, the optical properties seen in those plasmonic materials not only can be utilized to create new optical systems, also provide opportunities to cancer imaging and therapy [4]. The development of future phototherapy nanoagents just benefited from obtaining plasmon resonances in the near infrared, as these wavelengths are commonly used in biomedical fields [5, 6]. As the most common plasmonic materials, noble metals (such as Au and Ag) usually possess high carrier density and display apparent LSPR over a wide range from the ultraviolet (UV) region to NIR [7-10]. However, despite the easy manipulation of LSPR, noble metals inevitably suffer from earth rarity and their plasmonic frequencies are highly dependent on their sizes and shapes, as well as the surrounding mediums [11], which prevent them from being used in large scale practical applications.

Recently, it has been revealed that LSPR can also occur in some heavily doped semiconductor nanocrystals with an appreciable free carrier concentration. With respect to noble metals, the plasmonic resonance of semiconductors could be tailored by changing the stoichiometric compositions, dopant concentrations, or phase transitions. For example, copper chalcogenides [12, 13] and tungsten oxide[14] can obtain plasmon resonances in the visible and NIR regions, the creation of stable 2D semiconducting oxides of molybdenum is also revealed in Kalantar-zadeh's recent topical feature article[15]. Simply by irradiating the suspension of 2D flakes with solar energy in the presence of water, we induced oxygen deficiencies in the 2D flakes, which were completely stable both before and after the process. However, solar-light-driven process is one aspect that by controlling the oxygen vacancies in molybdenum flakes, active tuning of the plasmonic response in 2D molybdenum oxide [16]. In order to explore these unique plasmonic features in molybdenum oxides, in another aspect, accordingly, we explore tunable plasmonics in substoichiometric 2D molybdenum oxide nanoflakes

in the NIR range by mechanical exfoliating method. We show that these intercalating ions eventually take oxygen atoms from the exfoliating flakes, forming sub-stoichiometric molybdenum trioxide (MoO_{3-x}), which also displays a strong Prussian blue color and has ordered phases with a highly controlled stoichiometry.

The suspensions of 2D MoO_{3-x} nanoflakes are produced by using a facile two-step process (see the Experimental Section for details). In brief, the 2D MoO_3 flakes are first produced by hydrothermal of metal molybdenum powders with hydrogen peroxide in ethanol, then suffer from a liquid phase exfoliation method with a combination of mechanical grinding and sonication. Several unique properties of molybdenum oxide provide the key features to obtain a tunable 2D plasmon resonance in the NIR region. Therefore, we demonstrate the in vitro biomedical application of MoO_{3-x} NFs as photothermal reagents for the killing of Hela cells using 808 nm Laser. According to the results under the condition of hyperthermia when exposure to 808 nm realizing cancer ablation.

2. Experimental section

2.1 Materials and apparatus.

Molybdenum metal powder, hydrogen peroxide (H_2O_2, 30 wt %), ethanol, were purchased from Sigma-Aldrich Co. All chemical reagents were used without any further purification.

The morphology and size of the samples were observed on a field-emission scanning electron microscope (FE-SEM) (S-4800, Hitachi, Japan) and transmission electron microscopes (TEM, Tecnai G2 20 S-TWIN). The element analysis of the samples was performed by an energy-dispersive X-ray spectrum (EDX, HORIBA EMAX-250) attached on the FE-SEM. X-ray diffraction (XRD) analysis was performed using Japan Rigaku D/max-2500 diffractometer with Cu Kα radiation (λ=1.5418Å). X-ray photoelectron spectroscopy (XPS) was performed on a Kratos AXIS-165 surface analysis system. The UV-vis-NIR data were obtained by U-3900 spectrophotometer (Hitachi). The infrared thermal imaging was acquired at different irradiation time and recorded using a FLIR thermal camera (FLIR ThermaCAM E40).

2.2 Synthesis of MoO_3 Nanoflakes and then transfer to MoO_{3-x} Nanoflakes.

MoO_3 Nanoflakes were prepared by oxidizing metal molybdenum powders with hydrogen peroxide (H_2O_2,30%) followed by solvothermal treatment in ethanol solution at 160 ℃ for 12 h. In a typical synthetic procedure, 10 mmol of molybdenum metal powder was added to a round bottom flask (100 mL) containing 60 mL of ethanol. Then 15 mL of H_2O_2 was introduced and magnetically stirred for about 2 h to obtain the transparent yellow solution. This yellow precursor liquid were took out the 30 mL to a Teflon vessel and then sealed in stainless steel autoclave, heated and maintained at 160 ℃ for 12 h. After cooling down to room temperature naturally, the product was collected by centrifugation, rinsed with ethanol for three times and finally obtained through freeze-drying at vacuum.

30 mg of the obtained MoO_3 *Nanoflakes* powder was grounded with 0.6 mL acetonitrile for 30 min. The powder was then dispersed in a 50 vol% ethanol/water mixture (30 mL) probe sonicated (Ultrasonic Processor GEX500) for 12 h at the power of 125 W. Samples of MoO_{3-x} *Nanoflakes* aqueous solution were taken from at different point of time (0, 2, 6, 9, 12 h, respectively), and then centrifuged at 12000 rpm for 10 min at room temperature. The blue supernatant containing a high concentration of 2D molybdenum oxide flakes was collected and cast onto five small containers with 3 mL of the suspension in each of the five samples and were labeled as MNF-X (X=1，2，3，4，5).

2.3 NIR Photothermal Effect.

MoO_{3-x} Nanoflakes Sample-5 (MNF-5) water solutions with different concentrations were introduced into a quartz cuvette and irradiated by 808 nm NIR laser at a power density of 1.0 W/cm^2 for 10 min. To further measure photothermal conversion efficiency, 0.1 mg/mL of MNF-5 aqueous solution was introduced into a quartz cuvette and irradiated with 808-nm laser and then cooled to room temperature.

2.4 In vitro Cell Viability Assay of MNF-5.

Hela cells (a human cervical carcinoma cell line) were cultured with Dulbecco's Modified Eagle Medium (DMEM), respectively, which were supplemented with 10 % fetal bovine serum (FBS), at 37 ℃ in a humidified atmosphere with 5 % CO_2. The cell viabilities were evaluated by a standard Cell Counting Kit-8 (CCK-8) colorimetric assay. The three cells were seeded into 96-well culture plates (about 1×10^4 cells per well). After adding MNF-5 with different concentrations (3.125, 6.25, 12.5, 25, 50, 100, and 200 μg/mL), these cells were subsequently incubated with Hale cell for 24 h at 37 ℃ under 5% CO_2. Then, 10 % of CCK-8 medium solutions were added to each well and incubated for another 2 h. Finally, the absorbance was measured at 490 nm using SpectraMax M2 (MDC, USA). Six replicates were done for each treatment group.

2.5 In vitro Light-induced cytotoxicity of MNF-5 toward Cancer Cells.

Hela cells were cultured in a 96-well culture plate as a density of 1×10^4 per well for 12 h to allow the cell attachment. Solutions containing MNF-5 with different concentrations were added to the culture medium. After 4 h of co-incubation, Hela cells were irradiated by 808 nm lasers (1.0 W/ cm^2, 10 min) 37 ℃ and 4 ℃. Then, these cells were incubated for another 24 h and the cell viability was evaluated via a standard Cell Counting Kit-8 colorimetric assay.

2.6 Cellular Killing Ability.

Hela cells were chosen for investigating cell killing ability *in vitro*. The Hela cells were seeded in culture dishes (about 1×10^4 cells per well) overnight at 37 ^oC in a 5% CO_2. Then, the cells were incubated with MoO_{3-x} NFs (100 μg/ mL). After 24 h, the cells were washed by PBS. The cells incubated with MoO_{3-x} NFs were irradiated by 808 nm laser and 1064 nm laser at a power density of 1.0 W/cm^2 for 10 min, respectively. After 2 h, the cells were slightly washed by PBS and stained with calcein AM (CA) and propidium iodide (PI) for 15 min. The images were visualized by an inverted fluorescence microscope (OLYMPUS X-73, JAPAN).

3. Results and Discussion

In this synthetic process, the growth process of the MoO_{3-x} Nanoflakes was based on intrinsic growth. The solution-soluble precursor MoO_2 (OH)(OOH) under solvothermal treatments at elevated temperature (160 ℃) give birth to tiny MoO_3 nuclei by dehydration[17]. Due to the layered crystal structure of orthorhombic MoO_3, which is comprised of MoO_6 octahedra by sharing edges and corners, the intrinsic anisotropic crystal growth led to the preferential formation of 2D MoO_3 nanosheets. In addition, the stronger reducibility of ethanol enabled MoO_3 to be reduced for the formation of MoO_{3-x}. Therefore, upon solvothermal treatments for 12 h, well-defined 2D MoO_{3-x} nanosheets were obtained, followed by mechanical exfoliating that these intercalating ions eventually take oxygen atoms from the exfoliating flakes, forming sub-stoichiometric molybdenum trioxide (MoO_{3-x}), which also displays a strong Prussian blue color and has ordered phases with a highly controlled stoichiometry(Schematic 1).

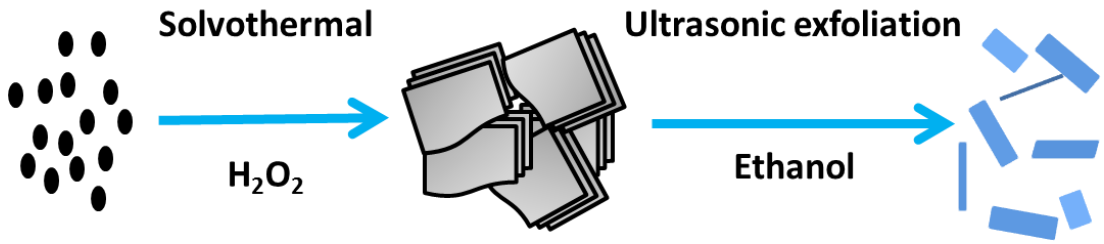

Sch. 1 Synthetic process of 2D Molybdenum Oxide Nanoflakes

Figure 1a presents the typical scanning electron microscopy (SEM) image of the as-prepared MoO_{3-x} nanoflakes products, from which numerous two-dimensional (2D) nanoflakes were observed. The diameter of the MoO_{3-x} nanoflakes ranges from 200 nm to 1mm, and the thickness is about 20-30 nm. Transmission electron microscopy image (TEM; Figure 1b) further confirms the products in the shape of nanoflakes. The formation of 2D MoO_{3-x} nanoflakes was considered to be associated with

the intrinsic growth of MoO_3 nuclei owing to the layered crystal structure, along with its reduction by ethanol at elevated solvothermal temperatures and exfoliating

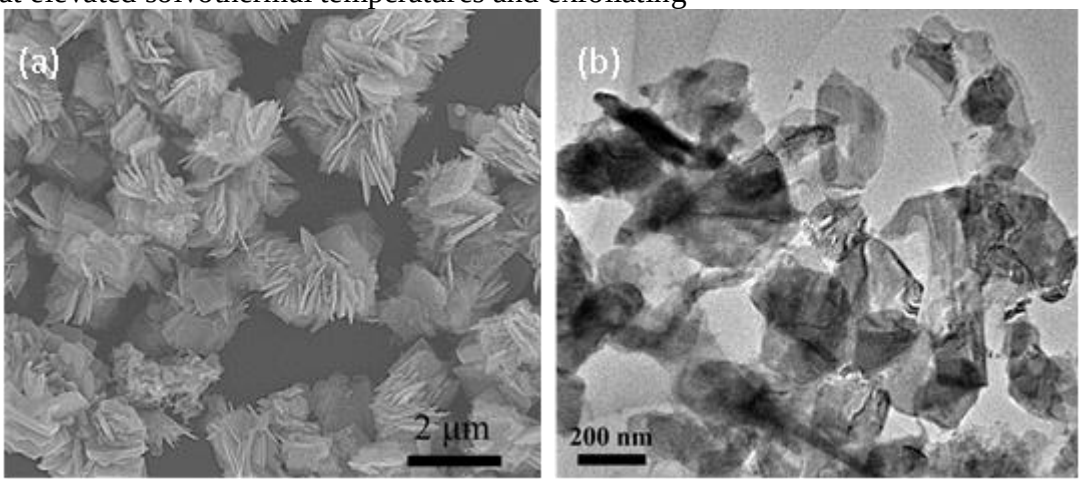

Fig.1 SEM and TEM image of the obtained MoO3-x Nanoflakes Sample-5 (MNF-5)
SEM image; (b) TEM image

From the X-ray diffraction pattern (XRD; Fig. 2), the product is assigned to the orthorhombic phase (JCPDS No. 5-0508), which is crystallized in a layered structure composed of MoO_6 octahedra by sharing edges and corners (inset).

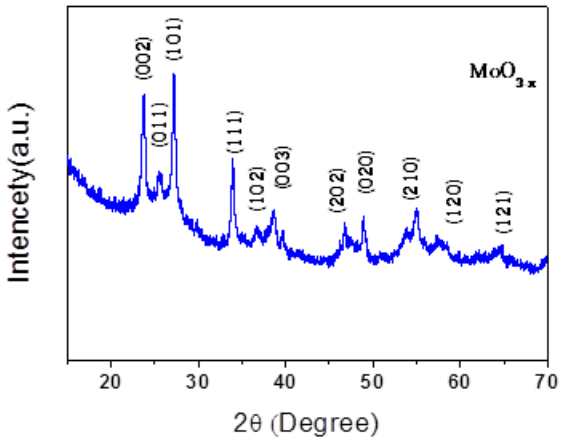

Fig.2 XRD patterns of the obtained MoO3-x Nanoflakes Sample-5 (MNF-5)

The EDX spectrum analysis manifested that the main elements of Mo and O can be detected and the well-defined distribution of molybdenum, oxygen, and carbon in 2D MoO_{3-x} nanoflakes (Fig. 3).

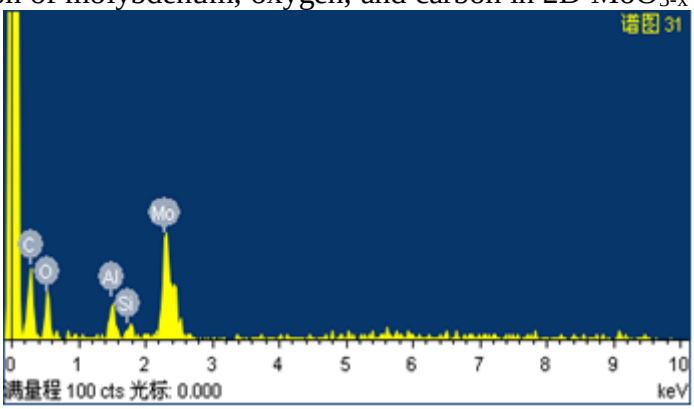

Fig.3 EDS patterns of the obtained MoO3-x Nanoflakes Sample-5 (MNF-5)

To elucidate the oxidation state of Mo in the plasmonic MoO_{3-x} nanostructures, X-ray photoelectron spectroscopy (XPS) measurements were carried out. Figure 4 displays the Mo 3d XPS core spectra of the as-prepared MoO_{3-x}. As can be seen, both Mo^{6+} and Mo^{5+} are present in the MoO_{3-x} nanoflakes.

For commercial MoO_3 sample, two peaks (232.6 and 235.7 eV) are attributed to the $3d^{5/2}$and$3d^{3/2}$of Mo6+, respectively [18]. In contrast, the peaks of Mo $3d^{5/2}$and $3d^{3/2}$shift to lower binding energies, and both of them can be divided into two separate peaks. The peaks at 232.6 and 235.7 eV correspond to Mo^{6+}, and those centered at 231.7 and 234.9 eV are assigned to Mo^{5+}[19]. According to the XPS peak area of Mo 3d, the Mo^{6+} and Mo^{5+}cations account for 22.7 % and 77.3 % of the total Mo states, respectively, in the MoO_{3-x} nanoflakes. The average oxidation state of Mo is thus determined to be 5.23, which is manifestly the mixed-valence state arising from the oxygen vacancies.

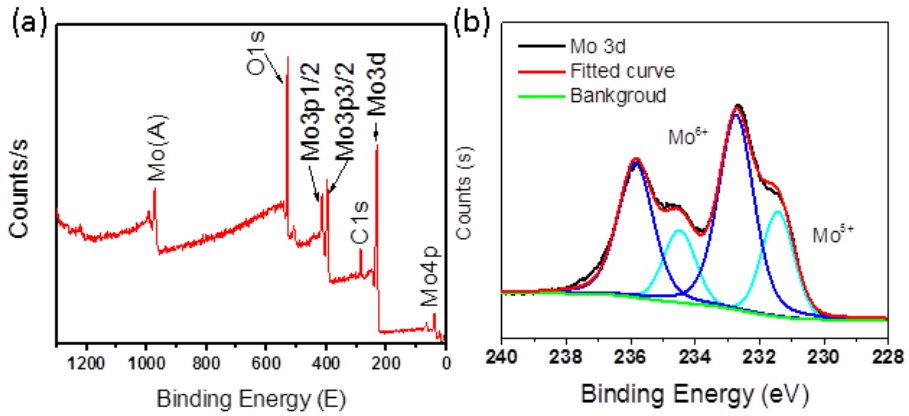

Fig.4 XPS spectras of the MoO3-x Nanoflakes

(a) XPS spectra of the MoO3-x Nanoflakes Sample-5 (MNF-5); (b) A survey XPS spectrum, and Mo3d core level spectrum

Figure 5 shows the UV/Vis–NIR spectra of the MNF-1~5. As can be seen, a strong absorption peak located at NIR associated with LSPR is clearly observed in the spectra of MoO_{3-x} nanoflakes. In addition, light-blue quasi-uniform molybdenum oxide nanoflakes with smaller sizes show remarkable improvement or deviation. As seen from the UV/Vis-NIR diffuse reflectance spectra, the corresponding LSPR peaks have obvious shifted, along with decreased absorption peak intensity, enables MoO_3 to generate more oxygen vacancies, thereby leading to deficient MoO_{3-x} with sufficient free carriers to support LSPR[20].

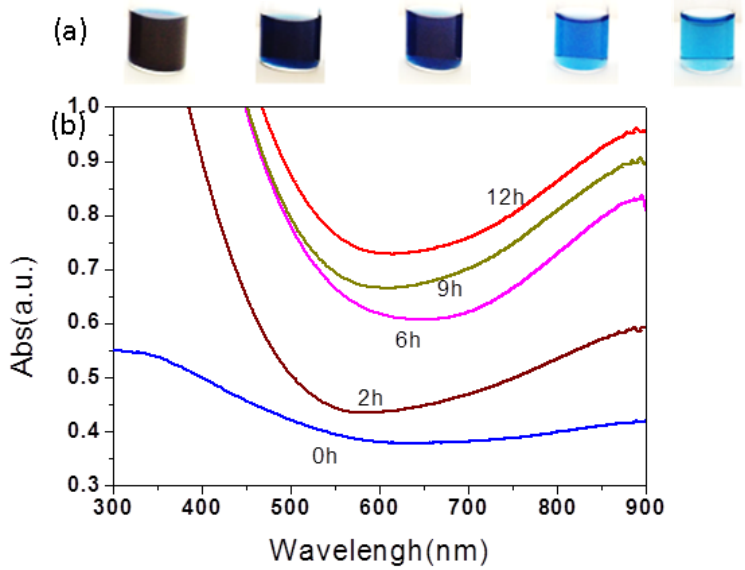

Fig.5 UV-Vis-IR absorption spectrum and the photographs of MNF1-5

(a) photograph of the products of different exfoliation time points; (b) UV-Vis-IR absorption spectrum of MNF1-5

Inorganic nanomaterials with many intriguing physical and chemical properties have shown great promise for cancer imaging and therapy[21]. Molybdenum oxide is no exception and the enhanced NIR absorption of MoO_{3-x} nanoflakes makes them promising candidates for photothermal agents. For

the determination of heating efficiency thermometry, we were able to measure the on-focus temperature increment (ΔT) (due to the heat delivered by the MoO_{3-x} NFs) as a function of the continuous laser power for 808 nm laser wavelengths used in this work. MoO_{3-x} NFs aqueous solution with different concentrations at 0.05, 0.1, 0.2, 0.4 and 0.5 mg/mL were introduced into a quartz cuvette and irradiated at a power density of 1.0 W/cm^2 for 10 min. As a blank control, temperature of deionized water increased to 27 ℃(1.0 W cm^2, 10 min), While all temperatures of MoO_{3-x} NFs aqueous solution increased fast and showed a concentration-dependent temperature increase, indicating these nanoparticles could efficiently convert laser energy into heat (Figure 6a).

To further measure photothermal conversion efficiency, 0.2 mg/mL of NFs aqueous solution was introduced into a quartz cuvette and irradiated with 808 nm laser, then cooled to room temperature. The conversion efficiency (η) is an important character for photothermal materials. To measure the photothermal conversion efficiency (η), the MoO_{3-x} NFs aqueous dispersion (0.2 mg/mL) were exposed to 808 nm CW laser (1W/cm^2) for 10 min, and then the laser was shut off. The heating and cooling temperature trends of samples were recorded by FLIR thermal camera (Fig. 6b). And, the photothermal conversion efficiency was calculated according to the eq. 1: [22]

$$\eta = \frac{hS\left(T_{max} - T_{surr}\right) - Q_0}{I\left(1 - 10^{-A_{808}}\right)} \quad (1)$$

Where *h* is the heat transfer coefficient, S is the surface area of the container, T_{max} is the steady state maximum temperature, T_{surr} is the ambient temperature of the surroundings, Q_0 is the baseline energy input by the solvent and the sample container without MoO_{3-x} NFs, I is the laser power, and A_{808} is the absorbance of MoO_{3-x} NFs solution at 808 nm. The value of hS is calculated by eq. 2:

$$\tau_s = \frac{m_d C_d}{hS} \quad (2)$$

Where τ_s is the characteristic thermal time constant, the mass of the m_d and C_d are the mass and heat capacity of water, respectively. The heat energy (Q_0) of the sample container and solvent without MoO_{3-x} NFs were measured independently using the eq. 3:

$$Q_0 = hS\left(T_{max} - T_{surr}\right) \quad (3)$$

Finally, the 808 nm laser induced photothermal conversion efficiency (η) of the MoO_{3-x} NFs was calculated as ~37.53%.

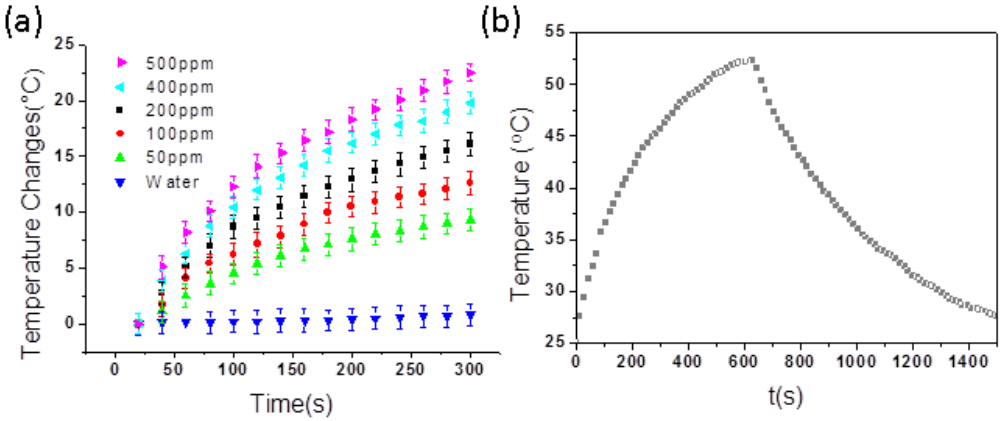

Fig.6 Photothermal effect of the of the MoO3-x Nanoflakes Sample-5 (MNF-5)

(a) Photothermal heating curves of pure water and MoO_{3-x} Nanoflakes in water with different concentrations under 808 nm laser irradiation at the power density of 1.0 W/cm^2; (d) Plot of cooling time versus negative natural logarithm of the temperature driving force which is obtained from the cooling stage

For safe bio-application of MoO_{3-x} Nanoflakes, Prior to using MoO_{3-x} Nanoflakes for in vivo usage, its biocompatibility and in vitro toxicity with living cells was investigated at first. Standard CCK-8 assay with the nanoparticles were performed on Hela cells. As illustrated in Figure 7, viability of the three cells was not hindered by these MoO_{3-x} Nanoflakes even up to a high concentration of 200 μg mL^{-1}. However, it leads to a drastic drop in the percentage of cell viabilities upon exposure to 808 nm light (1.0 W cm^{-2} for 10 min). This result indicates these samples are active in photo-induced cancer cell killing. Interestingly, the MoO_{3-x} Nanoflakes exhibits enhanced HeLa cell lethality in a dose-dependent manner compared with MoO_{3-x} Nanoflakes under the identical condition.

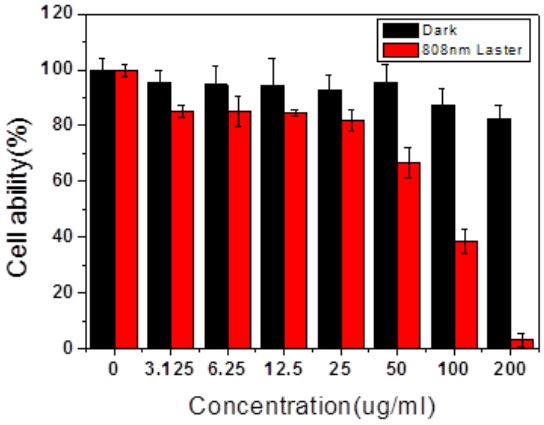

Fig.7 Cell viability of Hela cells treatment with MoO3-x nanoflakes with and with irradiation with 808 nm laser

To better elucidate the toxic effect of every individual element, when under 808 nm laser light irradiation, cell viabilities of HeLa cells with MoO_{3-x} Nanoflakes, a systematical study was carried out afterward. Neither NIR irradiation only group nor the specific concentration of single element groups could give rise to higher amount of cell death. Fluorescence images of Calcine AM/PI stained cells intuitively confirmed the effective killing of Hela cells (Fig. 8). It was noteworthy that more red dead cells without any cells were detected in the group of MoO_{3-x} Nanoflakes, indicating that MoO_{3-x} Nanoflakes under the 808 nm irradiation could cause more death of Hela cells.

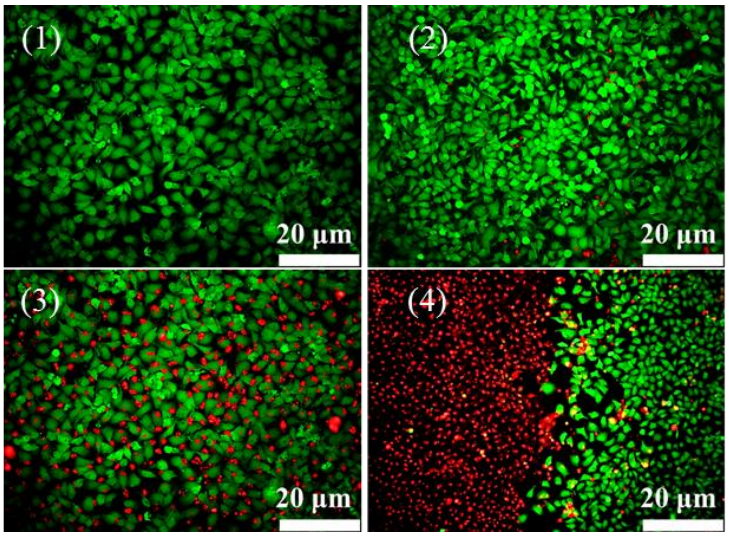

Fig.8 Fluorescence images of HeLa cells after co-staining using CA and PI
(1) Cells; (2) Cells+808 nm laser, (3) MoO3-x nanoflakes (100 μg/mL); (4) MoO3-x nanoflakes (100 μg/mL) +808 nm laser (Power density: 1.0 W/cm2)

4. Conclusion

In summary, well-defined 2D MoO_{3-x} nanoflakes were obtained by mechanical exfoliating method. The prepared MoO_{3-x} nanoflakes display strong LSPR in the NIR region, which increased along with the degree of exfoliation. In addition, the structural and optical stability of the MoO_{3-x} sample was further confirmed by XRD patterns and UV/Vis–NIR diffuse reflectance spectra before and after the exfoliation, which reveals the potential application of the plasmonic semiconductor nanostructures as efficient photothermal agent. This work illustrates a rational route to plasmonic MoO_{3-x} nanoflakes, which may offer a generalized method for generating other semiconductor nanostructures with LSPR, such as deficient vanadium and tungsten oxides. The further applications in the fields of destruction of solid tumors, in vivo bioimaging, and enzyme electron transfer reaction and so on are awaited investigation.

Acknowledgements

This work was supported by National Basic Research Programs of China (973 program, No. 2012CB932504 and 2015CB932104) and National Natural Science Foundation of China (No. 21177128, 21303200, 81472851).

References

[1] Faucheaux J-A, Stanton A-L, Jain P-K. Plasmon Resonances of Semiconductor Nanocrystals: Physical Principles and New Opportunities [J]. J Phys Chem Lett 2014, 5 (6), 976-85;

[2] Liu, Z.; Liu, X.; Ran, X.; Ju, E.; Ren, J.; Qu, X., Single-layer tungsten oxide as intelligent photo-responsive nanoagents for permanent male sterilization[J]. Biomaterials 2015, 69, 56-64;

[3] Bao, T.; Yin, W.; Zheng, X.; Zhang, X.; Yu, J.; Dong, X.; et al., One-pot synthesis of PEGylated plasmonic MoO(3-x) hollow nanospheres for photoacoustic imaging guided chemo-photothermal combinational therapy of cancer[J]. Biomaterials 2016, 76, 11-24.

[4] Ding, X.; Liow, C-H.; Zhang, M.; Huang, R.; Li, C.; Shen, H.; Liu, M.; et al., Surface plasmon resonance enhanced light absorption and photothermal therapy in the second near-infrared window[J]. J Am Chem Soc 2014, 136 (44), 15684-93.

[5] Dreaden, E-C.; Alkilany, A-M.; Huang, X.; Murphy, C-J.; Sayed, M-A., The golden age: gold nanoparticles for biomedicine [J]. Chem Soc Rev 2012, 41 (7), 2740-79;

[6] Vankayala, R.; Lin, C-C.; Kalluru, P.; Chiang, C-S.; Hwang, K-C., Gold nanoshells-mediated bimodal photodynamic and photothermal cancer treatment using ultra-low doses of near infra-red light [J]. Biomaterials 2014, 35 (21), 5527-38.

[7] Marinm B-C.; Hsum S-W.; Chenm L.; Lom A.; Zwisslerm D-W.; Liu Z.; et al.m Plasmon-Enhanced Two-Photon Absorption in Photoluminescent Semiconductor Nanocrystals [J]. ACS Photonics 2016;

[8] Vankayala, R.; Huang, Y. K.; Kalluru, P.; Chiang, C. S.; Hwang, K. C., First demonstration of gold nanorods-mediated photodynamic therapeutic destruction of tumors via near infra-red light activation[J]. Small 2014, 10 (8), 1612-22;

[9] Thangaraju, M-P.; Mehala, R., Novel Classification based approaches over Cancer Diseases [J]. Ijarcce 2015, 294-297.

[10] Cheng, L.; Wang, C.; Feng, L.; Yang, K.; Liu, Z., Functional nanomaterials for phototherapies of cancer[J]. Chem Rev 2014, 114 (21), 10869-939.

[11] Hsu, S.-W.; Bryks, W.; Tao, A. R., Effects of Carrier Density and Shape on the Localized Surface Plasmon Resonances of Cu2–xS Nanodisks[J]. Chemistry of Materials 2012, 24 (19), 3765-3771.

[12] Wu, Z-C.; Li, W-P.; Luo, C-H.; Su, C-H.; Yeh, C-S., Rattle-Type Fe3O4@CuS Developed to Conduct Magnetically Guided Photoinduced Hyperthermia at First and Second NIR Biological Windows [J]. Adv Funct Mater 2015, 25 (41), 6527-6537;

[13] Poliraju, Kalluru.; R,. V.; Chi-Shiun, Chiang.; Kuo Chu Hwang., Photosensitization of Singlet Oxygen and In vivo Photodynamic Therapeutic Effects Mediated by PEGylatedW18O49 Nanowires[J]. Angew. Chem. Int. Ed. 2013, (52), 1-6;

[14] Murray, W-A.; Barnes W-L., Plasmonic Materials[J]. Adv Mater 2007, 19 (22), 3771-3782;

[15] Song, G.; Shen, J.; Jiang, F.; Hu, R.; Li, W.; An, L.; et al., Hydrophilic molybdenum oxide nanomaterials with controlled morphology and strong plasmonic absorption for photothermal ablation of cancer cells[J]. ACS Appl Mater Interfaces 2014, 6 (6), 3915-22.

[17] Hu, J.; Tang, Y.; Elmenoufy, A-H.; Xu, H.; Cheng, Z.; Yang, X., Nanocomposite-Based Photodynamic Therapy Strategies for Deep Tumor Treatment[J]. Small 2015, 11 (44), 5860-87.

[18] Bhosle, V.; Tiwari, A.; Narayan J.,Epitaxial growth and properties of MoO[sub x](2<x<2.75) films[J]. J Appl Phys 2005, 97 (8), 083539.

[19] Liu, B.; Zhao, X.; Xiao, Y.; Cao, M., High-surface-area F-doped amorphous MoOx with high-performance lithium storage properties [J]. J Mater Chem A 2014, 2 (10), 3338.

[20] Song, G.; Hao, J.; Liang, C.; Liu, T.; Gao, M.; Cheng, L.; et al., Degradable Molybdenum Oxide Nanosheets with Rapid Clearance and Efficient Tumor Homing Capabilities as a Therapeutic Nanoplatform[J]. Angew Chem Int Ed Engl 2016, 55 (6), 2122-6;

[21] Seidl, C.; Ungelenk, J.; Zittel, E.; Bergfeldt, T.; Sleeman, J. P.; Schepers, U.et al., Tin Tungstate Nanoparticles: A Photosensitizer for Photodynamic Tumor Therapy[J]. ACS Nano 2016, 10 (3), 3149-3157.

[22] Geng, Ku.; Min, Zhou.; Shaoli, Song.; Qian, Huang.; John, Hazle.; Chun, Li., Copper Sulfide Nanoparticles As a New Class of Photoacoustic Contrast Agent for Deep Tissue Imaging at 1064 nm[J]. ACS Nano 2012, 6 (8), 7489–7496.